Stochastic Epidemic Outbreaks: Why Epidemics Are Like Lasers

Ira B. Schwartz[a] and Lora Billings[b]

[a]US Naval Research Laboratory, Code 6792, Washington, DC 20375 USA
[b]Montclair State University, Department of Mathematical Sciences, Montclair, NJ 07043 USA

ABSTRACT

Many diseases, such as childhood diseases, dengue fever, and West Nile virus, appear to oscillate randomly as a function of seasonal environmental or social changes. Such oscillations appear to have a chaotic bursting character, although it is still uncertain how much is due to random fluctuations. Such bursting in the presence of noise is also observed in driven lasers. In this talk, I will show how noise can excite random outbreaks in simple models of seasonally driven outbreaks, as well as lasers. The models for both population dynamics will be shown to share the same class of underlying topology, which plays a major role in the cause of observed stochastic bursting.

1. INTRODUCTION

One of most fascinating problems in populations dynamics is that of predicting the origin of large amplitude events in environments which are random. Examples come from the field of biology (coupled neurons),[1] epidemiology (random outbreaks and pandemics),[2–4] and optics (lasers).[5] In many examples where large numbers of individuals or particles are assigned states in fluctuating environments, the dynamical processes are far from equilibrium. Such is the case when there exists a fluctuating force driving the system, causing any equilibria to be time dependent.

Historically, an interesting set of examples of noise induced large amplitude events comes from the overlap of physics and biology. Charles Townes, in his memoir dealing with the development of the laser, describes his interaction with with a biologist while visiting the University of Tokyo.[6] In particular, he states that they wanted to account for the appearance of photons in a maser, resulting in a meeting with several colleagues to study the population fluctuations of microbes. Based on these studies from population biology, Townes and his co-workers developed a precise theory of random fluctuations in masers. It is one of the few examples illustrating an application from biology creating new ideas in physics.

In epidemics, it is clear that fluctuations play a major role in determining outbreaks which occur in both local and global geographic areas. In Ref. 4, major outbreaks throughout history have been recorded, such as the bubonic plague in 14th century Europe (25 millions deaths) and 1685 London (68,000 deaths), and the pandemic influenza of 1921 (20 million deaths). More recently, measles worldwide (1 million deaths) is still a hotbed issue for those who are trying to develop vaccines.

Models of epidemics throughout history have been designed not only describing the past, but with the hope of predicting new outbreaks in the future. In Ref. 7, we find the very early reference to the 1760 paper by Daniel Bernoulli who was developing smallpox models with the goal of affecting public policy. Other early contributions are known as well,[4] but one of the most important contributions for the purposes of this paper is the first development by Hamer[8] of the notion that there is a contact rate between infectives and susceptibles. For the time period alone, this was remarkable since it was the first idea of introducing a nonlinear term into any of the population models. It is still widely used today.[9]

Although much modeling has been done to explain and predict outbreaks, there still is a large gap between theory and data. In general, testing epidemic prediction is close to impossible due to the social nature of populations and incomplete and inaccurate data recording. Such inaccuracies in data make models and parameters estimation far from quantitative. Therefore, the question we consider is one which asks whether laser models and experiments, which are quantitative, capture the same dynamics as epidemic outbreaks. To address the
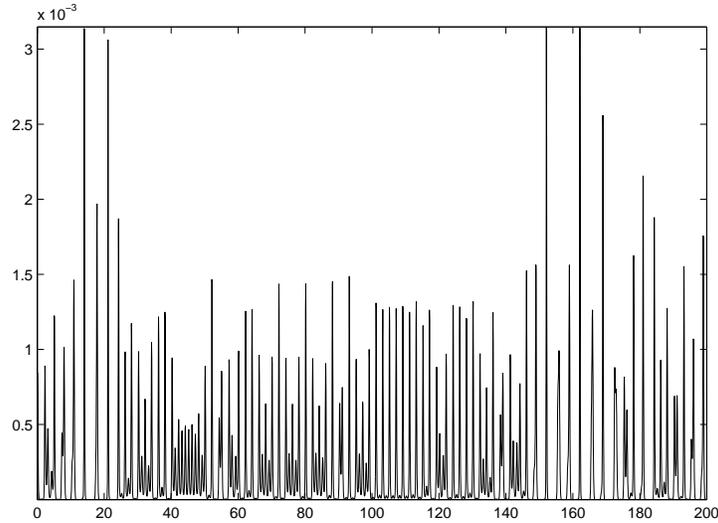
Figure 1. Example of a seasonally driven stochastic SEIR epidemic model. Plotted is the fraction of infective as a function of time (years). The SEIR model given by Eq. (2).

question, we will consider two classes of models from lasers and epidemics, and show that they share similar dynamics based on perturbations of a Hamiltonian system which has Hamiltonian

$$H(x, y) = e^x - x + \frac{y^2}{2} + 1. \tag{1}$$

Explanations of how outbreaks occur in an ideal dynamical system will be shown based on Eq. (1), and how local and global bifurcations arise when considering the details of the laser and epidemic models. As a result of the dynamical structure, we will also show how the topology is almost identical for the two systems. Including noise in the topological structure will then induce chaotic looking outbreaks in both systems. By examining such a system probabilistically, one can then make predictions based on transition probabilities, and compare with data. Such system identification is ripe for control, and we will close with an example of how to optimize outbreak prediction above a threshold.

1.1. Time series comparison

Epidemics that are time dependent oscillate randomly. In particular, if they are driven seasonally, or with regular gatherings of population subgroups, the period between outbreaks may be regular, but the amplitudes will appear to be random.[10, 11] Such is the case in childhood diseases in the UK, New York, and Baltimore in the pre-vaccine era. General characteristics of the outbreaks that are observed are: 1. They are time dependent. 2. Oscillate randomly. 3. Large outbreaks are usually followed by several low years. 4. Sociological parameters, such as birth rates and contact between individuals, are non-stationary. Such observations have led to many people believing the outbreaks are chaotic, meaning that they are derived from a deterministic process.[12] However, it is clear from data observations that there must indeed exist random fluctuations that affect the outbreaks. An example from an SEIR stochastic model that is seasonally driven and exhibits many of the characteristics of the data mentioned above is given in Fig. 1.

To examine the outbreaks in the epidemic against a physical system, one can compare it to experimental data from a stochastically driven CO_2 laser, shown in Fig. 2. The similar features listed above for the epidemic model simulation can be clearly seen the laser experiment. Therefore, we are motivated to derive a theoretical framework that encompasses both epidemic and laser stochastic dynamics.
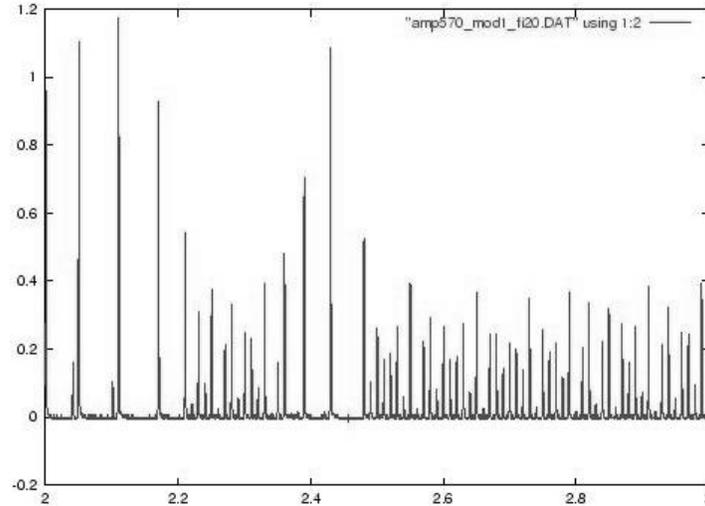
Figure 2. Laser intensity from a CO_2 laser experiment as a function of time. The units are arbitrary.

2. POPULATION MODELS

In order to compare the dynamics of the laser and epidemic models, we consider the problems to be posed in a periodically fluctuating environment, but with additive noise. For model derivations and a full description of the details see Refs. 13–15.

2.1. Epidemic model

We consider modeling a population to consist of fractions of susceptibles, S, exposed, E, infectious, I, and recovered, R, individuals, such that they sum to unity for all time. The model equations, known as the SEIR model, are given by the following rate equations:

$$
\begin{aligned}
S' &= \mu - \beta(t)IS - \mu S \\
E' &= \beta(t)IS - \alpha E - \mu E \\
I' &= \alpha E - \gamma I - \mu I \\
R' &= \gamma I - \mu R
\end{aligned} \quad + \vec{\eta}(t),
\tag{2}
$$

where periodic forcing is given by $\beta(t) = \beta_0(1 + \delta cos(2\pi t))$, μ is the birth and death rate, α^{-1} is the mean latent period, γ^{-1} is the mean infectious period, and $\vec{\eta}$ is a random noise vector having normal distribution and mean zero. Much analysis has been done on Eq. (2), and we refer the reader to Refs. 3, 4, 15–17 for just some of the papers.

2.2. Laser Model

The laser model we use models a CO_2 laser as a 4 level system.[18] Here the rate equations are given by:

$$
\begin{aligned}
I' &= [g(N_2 - N_1) - k_0(t)]I \\
N_1' &= -(z\gamma_r + \gamma_1)N_1 + g(N_2 - N_1)I + \gamma_r M_1 \\
N_2' &= -(z\gamma_r + \gamma_2)N_2 - g(N_2 - N_1)I + \gamma_r M_2 + \gamma_2 P \\
M_1' &= -(\gamma_r + \gamma_1)M_1 + z\gamma_r N_1 \\
M_2' &= -(\gamma_r + \gamma_2)M_2 + z\gamma_r N_2
\end{aligned} \quad + \vec{\eta}(t),
\tag{3}
$$

where I is the intensity, N_1 and N_2 are the main energy levels, and M_1 and M_2 are rotational sub-levels. The loss term is $k(t) = k_0(t + T)$, where T is the period of the drive. Noise is assumed to be additive here, as in Eq. (2). For details about parameters values in the model and experiment, see Ref. 19.

2.3. A model comparison

If one assumes the models in Eqs. (2) and (3) have no periodic forcing and no noise, then one can show that the steady states that form a slow buildup of both populations, namely inversion and susceptibles, and satisfy the approximate relationships:

$$N_- = N_2 - N_1 = \frac{k_0}{g} \quad \text{and} \quad S = \frac{\gamma}{\beta_0}. \tag{4}$$

The interpretation is that at steady state, there is a balance between the loss rates and the gains due to nonlinear contacts. In Eq. (2), it is the ratio of infectious rate to contact rate, while in Eq. (3), it is the ratio of loss to the laser gain. As a result of the analogy, one can find a direct correspondence between parameters, which we list in Table 1. When examining both models, from the table one can see that there exist two main drivers of the intensity of the laser and infectives of the SEIR model: One is the input terms, corresponding to the pump of the laser, and birth rate of the population. The other important term is the mass action coefficients, which generate the nonlinearity in each of the models.

Table 1. Table of parameters

Main laser parameters	Main epidemic parameters
g - gain	β_0 - contact rate
k_0 - dissipation rate	γ - infectious rate
P - pump rate	μ - birth rate

Based upon the parameter comparison, as well as competing time scales, one can cast both models in terms of a perturbed system based upon the Hamiltonian in Eq. (1). The transformations to get the results are complicated, but an idea of how to achieve the derivations may be found in Ref. 13. Here, we just list the results in terms of a perturbed system. In both models, we introduce a small parameter, ϵ, which is different in both model parameters, but for the purposes here, is a dimensionless parameter which scales the equations to the following:

Scaled laser equations:

$$
\begin{aligned}
y_1' &= \frac{\partial H(y_1, y_2)}{\partial y_2} \\
y_2' &= -\frac{\partial H(y_1, y_2)}{\partial y_1} + \epsilon(g_1(y_1, y_2, y_3) + f_1(t)) \\
y_3' &= \epsilon(g_2(y_1, y_2, y_3) + f_2(t)).
\end{aligned}
\tag{5}
$$

Scaled SEIR equations:

$$
\begin{aligned}
y_1' &= \frac{\partial H(y_1, y_2)}{\partial y_2} + \epsilon h_1(y_1, y_2, y_3, t) \\
y_2' &= -\frac{\partial H(z, y_2)}{\partial y_1} + \epsilon h_2(y_1, y_2, y_3, t) \\
\epsilon y_3' &= -\kappa y_3 + \epsilon h_3(y_1, y_2, y_3, t)
\end{aligned}
\tag{6}
$$

The dependent variables y_2 and y_1 are scaled versions of infectives (intensity) and susceptibles (inversion), respectively. Since ϵ is considered to be a small parameter, both Eqs. (5) and (6) are perturbations of a Hamiltonian system. However, there is one major difference between the two scaled models. In Eq. (5), the perturbation of the third equation is a regular perturbation, while in Eq. (6), the perturbation comes in the form of a singularly perturbed equation. In both cases, however, the perturbations allow a further reduction to a two dimensional system that is periodically driven, and has additive noise.
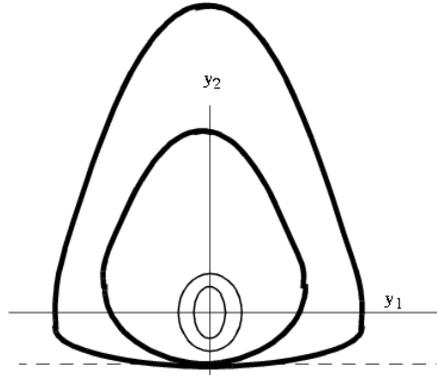
Figure 3. A picture of of periodic orbits of the Hamiltonian system.

Since the systems have a first integral when ϵ is zero, the origin is a center (which is now the steady state for both systems), but the manifold $y_2 = -1$ is invariant, as shown in Fig. 3. Therefore, for large energy levels, orbits spread out along the invariant manifold of the conservative system, and near that manifold, the dynamics is on a slow time scale. The infectives (or intensity) is very low here, and once the slow increase of susceptibles (or inversion) builds up to a critical level, the system switches to a fast time scale accompanied by a large jump in infectives. Thus, from the Hamiltonian system shared by the two models, one can see how an ideal outbreak occurs.

3. LOCAL AND GLOBAL BIFURCATION

In the presence of small ϵ and periodic forcing, one may use the Hamiltonian system to prove the existence of local bifurcations. In particular, one can have local bifurcations that are small amplitude oscillations near the center, and one can use the large amplitude periodic orbits in Fig. 3 to perturb from to show the existence of large amplitude oscillations which emanate from saddle-node bifurcations.[20] For the two systems considered here, one can prove the following statements:

Given an N-periodic orbit of the Hamiltonian system, then for the perturbed systems:

1. There exist parameter values of Eqs. (5) and (6) such that there exists a saddle-node pair of orbits of period N.

2. There exists a range of parameters in which bi-stability occurs where both small and large amplitude oscillations co-exist.

3. There exists a region of bi-instability, in which *unstable* orbits co-exist.

Such a result is important when we consider the effects of noise on the dynamics. To see an explicit example of the results, bifurcation Fig. 4 was computed for a reduced laser system.[20] Notice that there are regions of bi-stability and bi-instability. Bi-instability of small amplitude and large amplitude bursts will play a significant role in the predicting the effects of noise.

4. TOPOLOGICAL DYNAMICS - THE GLOBAL PICTURE

¿From the scaled Eqs. (5) and (6), one can eliminate the variable y_3 and reduce both systems down to a two dimensional periodically forced (period 1) stochastic system. We now consider the general problem of examining the interaction of noise and manifolds. Since the system is periodically driven, we consider a Poincaré section as a two-dimensional map, F, of a region D in the plane into itself, perturbed by stochastic components:

$$\vec{z}(t+1) = F\left[\vec{z}(t)\right] + \vec{\eta}(t), \tag{7}$$
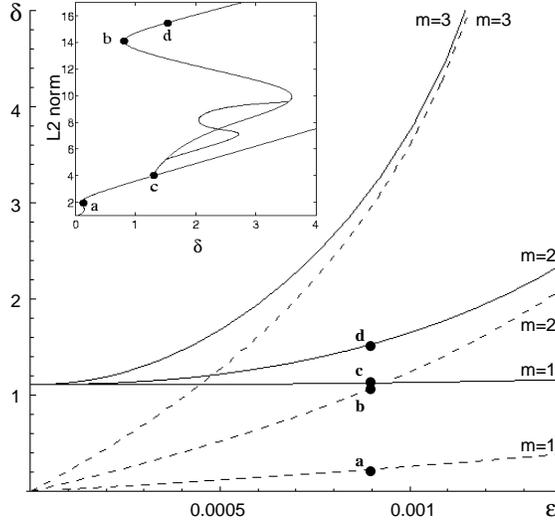
Figure 4. The figure show the branches of excited periodic orbits as a function of drive amplitude, δ and ϵ. From the inset, which shows the norm of the solution as a function of δ for a fixed ϵ, there exist two attracting and two unstable co-existing orbits between labels c and d.

where $\vec{\eta}$ is a two-dimensional random variable having a normal distribution given by

$$v(x) = e^{-(x^T \Sigma^{-1} x)/2} \big/ (2\pi \|\Sigma\|^{1/2}), \tag{8}$$

with $\Sigma = diag(\sigma^2)$.

We first consider the no noise case topology. From the bifurcation picture in Fig. 4 and the fact that the problem is now restricted to two-dimensions, the deterministic picture of the manifolds in the bi-stable region is expected to look like Fig. 5.[20] In particular, there is no complete topology that will generate a chaotic attractor or chaotic saddle. There do exist heteroclinic points, but they are only in the forward direction. As a a result, there exist complicated looking transients, but almost all initial conditions will converge to one of two periodic attractors. Because there is no reverse connection, there is no chaotic saddle, so there is no chaotic transient.

For the two models considered here, we have exactly the same structure in a bi-stable regime, pictured in Figs. 6 and 7. In Fig. 7, the bursting solution having large peaks is a large amplitude (LA) period 2 attractor, which lies in the gray basin region. (Note that we use SA for *small amplitude.*) In Fig. 7, the bursts are outbreaks associated with the large amplitude period 3 attractor. It is a remarkable fact that since the systems in Eqs. (5) and (6) share the same Hamiltonian structure and different perturbations, they still possess the same global topology. Moreover, the stable manifold associated with the LA saddle in each case forms the basin boundary, separating the large amplitude attractors from those that are small.

5. THE INTERACTION OF TOPOLOGY AND NOISE

In the generic case of Fig. 5, it is clear that in the bi-stable regime, there exist two distinct basins of attraction, which are analogous to potential wells. When adding noise, therefore, the problem becomes one of finding regions of escape from a basin. For one dimensional autonomous systems with additive noise, there exist results which show multiple attractors give rise to noise induced escape from one attractor to another. Such systems may be analyzed by considering escape from attracting potential wells along most probable exit paths as in Ref. 21, using the theory of quasi-potentials,[22] or a variational formulation of optimal escape paths.[23, 24] However, here we are interested in making prediction based not on paths of escape, which is in general good for small noise, but when do future large amplitude bursts, or outbreaks, occur based on current observations. To do this, we turn to the machinery of the stochastic Frobenious Perron operator.
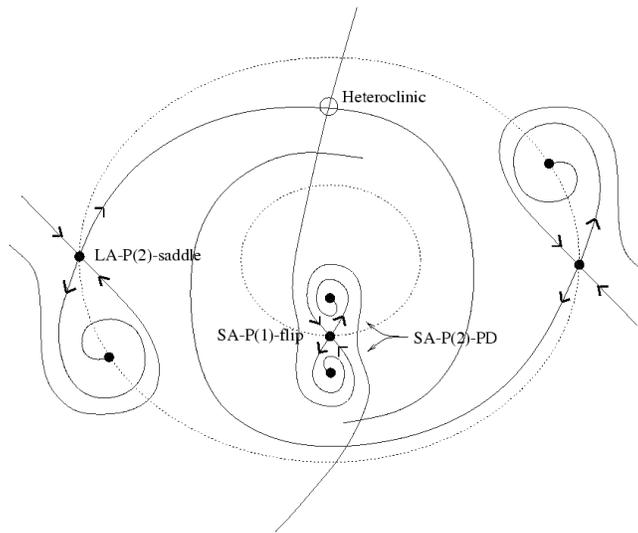
Figure 5. A generic picture of the global topology in the bi-stable regime lying between labels c and d in Fig. 4. LA stands for *large amplitude*, SA for *small amplitude*. Shown are a LA period 2 saddle, a small amplitude period one flip saddle, a small amplitude period 2 attractor, and LA period 2 attractor. Notice that the stable manifold of the SA period one saddle intersects the stable manifold manifold of period 2 LA saddle, forming a one way heteroclinic connection.
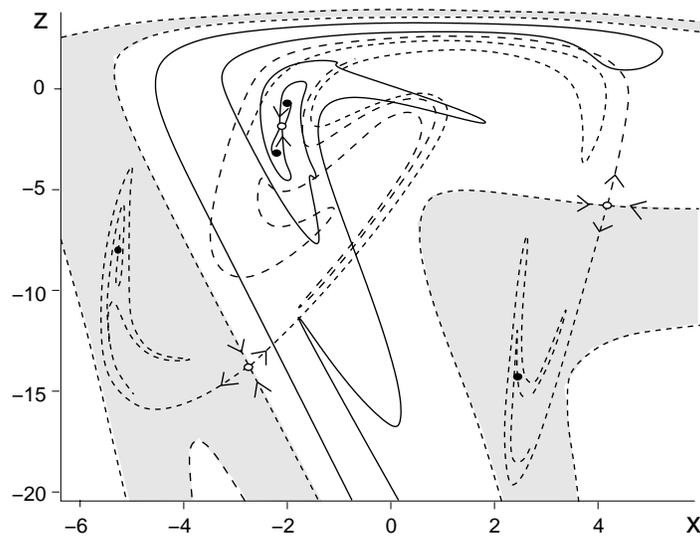
Figure 6. Manifolds and basin of attraction of a 2D reduced laser model. The large amplitude period 2 lies in the gray basin region. Almost all other points in white converge to the small amplitude period attractor. The stable manifold of the LA period 2 saddle forms the basin boundary separating the large and small attractors.
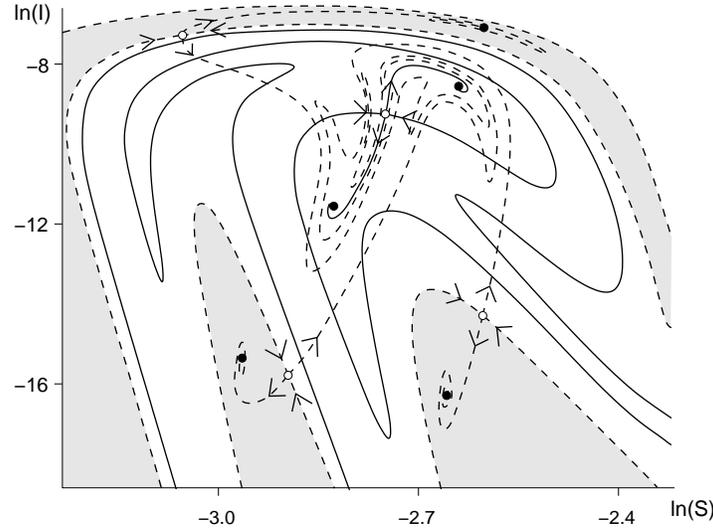
Figure 7. Manifolds and basin of attraction of a 2D reduced epidemic model. The large amplitude period 3 lies in the gray basin region. Almost all other points in white converge to the small amplitude period 2 attractor. The stable manifold of the LA period 3 saddle forms the basin boundary separating the large and small attractors.

If the noise is continuous, we can compute the evolution of the probability density using a Fokker-Planck approach.[25] However, since the approach here is one of discrete noise as in Eq. (7), we evolve the densities discretely as well. That is, since the solution to the periodically driven system is computed every period to form the discrete map, we do the same with the density. It is also a more direct theory of the interaction between noise and topology.

We assume the noise comes from a distribution, $\nu(x)$. The evolution of an initial probability density function (PDF), $\rho : D \subset \Re^2 \to \Re$, is defined by the stochastic Frobenius-Perron operator,[14] given by

$$P_F[\rho(x)] = \int_D \nu(x - F(y))\rho(y)dy. \tag{9}$$

The density is invariant if it is a fixed point of the operator. This approach allows an approximation of the probabilistic transitions of one part of phase space to another[14] as well as the invariant density.[26] To compute the transition probabilities from one region of phase space to another, we discretize the region D of phase space. Specifically, we assume there exists a cover of the region D by the union of the closure of disjoint open rectangles B_i,

$$D = \bigcup_{i=1}^{N} cl(B_i). \tag{10}$$

Defining the set of characteristic basis functions,

$$\psi_i(x) = \chi_{B_i}(x) \equiv \left\{ \begin{array}{l} 1, \ x \in B_i \\ 0, \ x \notin B_i \end{array} \right. \tag{11}$$

allows one to generate finite dimensional projections of transport by computing the $N \times N$ matrix entries of a transition probability matrix[14, 27] given by the equation

$$M_{i,j} = \int_D P_F(\psi_i(x))\psi_j(x)dx. \tag{12}$$

Therefore, Eq. (12) yields exactly the probability of transporting mass from box B_i to B_j, upon iteration of the stochastic dynamics. With the matrix in hand, we can then compute the conditional probability of going from
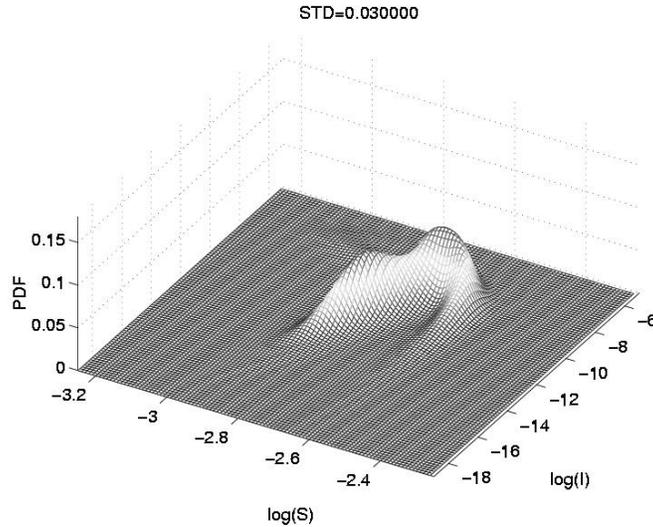
Figure 8. The invariant density for the epidemic model when the standard deviation is 0.03. At this value of noise, the system has gone through a bifurcation, and exhibits chaos-lke behavior.

a small amplitude observation to a large outbreak. We define this as probability flux transport. Moreover, fixed points of the stochastic Frobenious Perron operator are just the invariant density, and therefore, the eigenvector of the transition probability matrix having eigenvalue unity is the approximate invariant PDF of the system. From the epidemic model, an example of the invariant density is shown in Fig. 8 for noise which is strong enough for sufficient mixing between large and small amplitude outbreaks. Notice that if the noise was small, the small amplitude period attractor would be close to two peaks centered on the period 2 fixed points.[27] In contrast, for the standard deviation shown in Fig. 8, the noise spreads the density along an the unstable manifolds and stable manifolds, where unstable contributions to the local averages can be found.

The invariant density gives the distribution one sees for the stochastic attractor, but does not necessarily give the explicit future prediction. For that, we can use the transition probability matrix. For the noise level used in Fig. 8, we show the associated transition matrix in Fig. 9. The block diagonal elements are those entries corresponding to boxes which stay in the respective basins. That is, the upper diagonal elements are those boxes which remain in the small amplitude period 2 basin, while the lower diagonal entries are those remaining in the large amplitude basin. The upper right corner are those entries which have a measurable probability of transitioning from small to large amplitude outbreaks, and conversely for the lower left corner. The lines separating the block diagonals represent, therefore, the basin boundaries, or the stable manifolds connected to the period 3 saddle.

Given the transition probability matrix for both lasers and epidemics, one can convert the probabilities back to phase space, and examine regions of highest transition to a large outbreaks. The computational results are illustrated in Figs. 10 and 11. In both cases of the laser and epidemics, we have combined the flux transport results with the manifolds to illustrate where the systems transport most of probability. Notice that in both cases, regions near the large amplitude saddles contain sufficient probability to make the transition from a SA to LA outbreak. However, it is important to notice that the maximum regions of transport do not always lie near the saddles, but rather may be determined by the proximity of stable and unstable manifolds to each other, as shown in the high probability transport region in Fig. 10.

6. CONCLUSIONS

We have compared a class of population models driven by noise on both a local and global topological scales. The two population models, one from epidemiology and one from laser physics, were shown to share a common
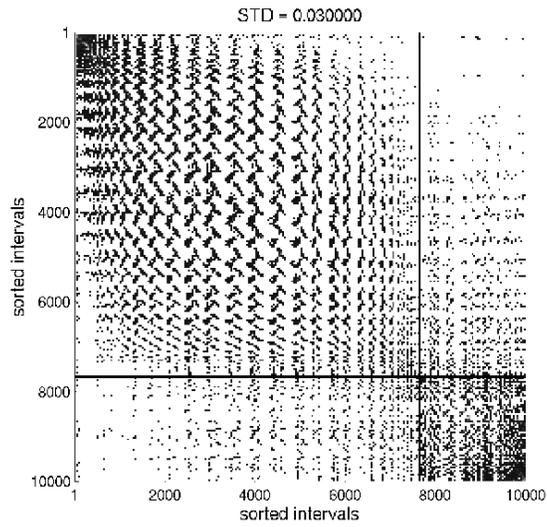
Figure 9. The transport matrix for a standard deviation of 0.03 in the epidemic model. The upper right corner designates those boxes which have measurable probability of transitioning from a small amplitude oscillation to a large amplitude outbreak.
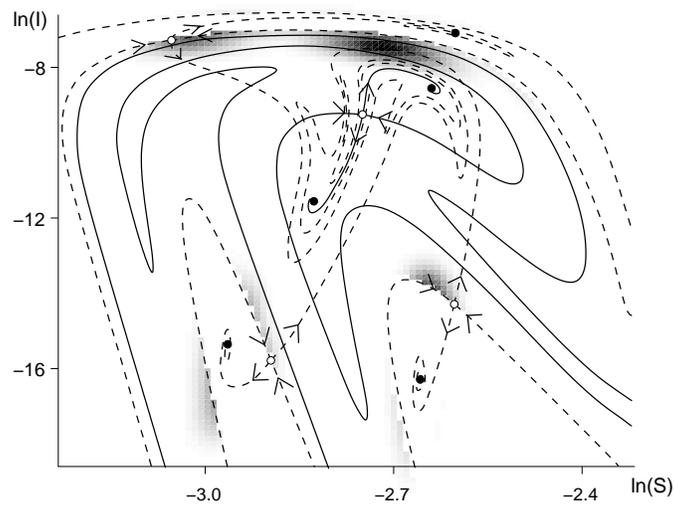
Figure 10. The transition probability from small to large amplitude outbreaks for the epidemic model.
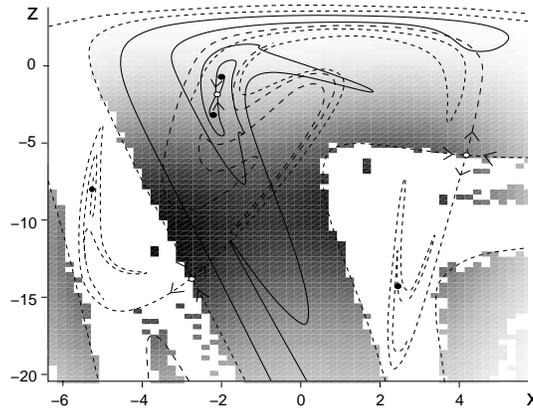
Figure 11. Transition probability from small to large intensity bursts for the laser model.
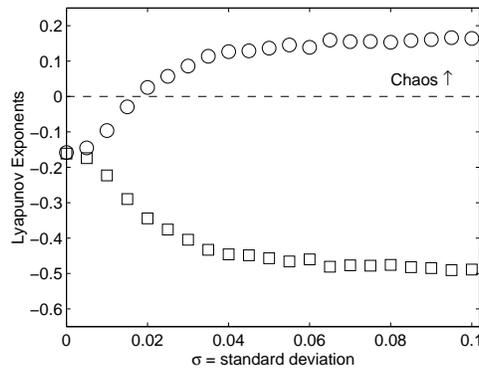
Figure 12. Lyapunov exponents for the epidemic model as a function of standard deviation of the noise distribution. A P-type bifurcation occurs when the maximum Lyapunov exponent passes through zero to become positive.

underlying Hamiltonian structure. Although the small perturbation terms are different for both systems,[13] the topological picture is the same.

When noise is added, it is interesting that there is no chaotic saddle to excite. Nonetheless, the transport from one basin to another predicted by the stochastic Frobenious Perron operator formalism shows that for sufficient noise levels large amplitude outbreaks are excited. Moreover, the dynamics, as a result of the stochastic terms, begins to sample the underlying stable and unstable manifold structures defined by the deterministic part of the models. One might expect that since the observed time series has random looking large amplitude events, the dynamics looks like a chaotic structure even though it is stochastic. Some evidence of this comes from the invariant density from the stochastic Frobenious Perron operator in Fig. 8. A more concrete computation would be that of a positive Lyapunov exponent, which would indicate a phenomenal, or P-type, bifurcation.[28] Since we already have an invariant PDF for the stochastic attractors of Eqs. (5) and (6), we can compute the Lyapunov spectrum using spatial averages, assuming the ergodic hypothesis holds. In Figs. 12 and 13, we show the transition to a P-type bifurcation as the standard deviation increases. It is interesting to note that the transition is smooth, which may be interpretted as the dynamics sampling more unstable parts of the manifold structure as the standard deviation is increased.

Finally, we discuss how one might optimize the predictions for epidemic outbreaks generated by the high probability regions in Fig. 10. Probailistic predictions based on the stochastic Frobenious Perron operator, and in general, are dependent on which regions one monitors. In the epidemic model, we consider the highest
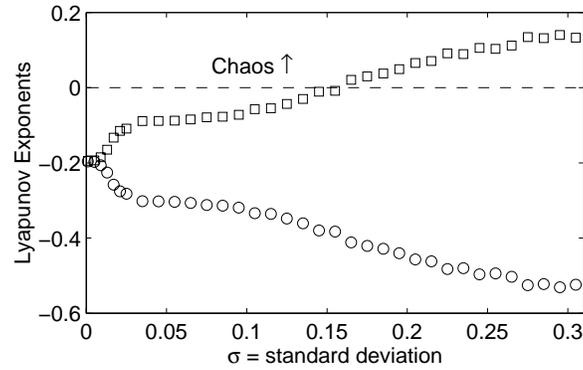
Figure 13. Lyapunov exponents for the laser model as a function of standard deviation of the noise distribution.
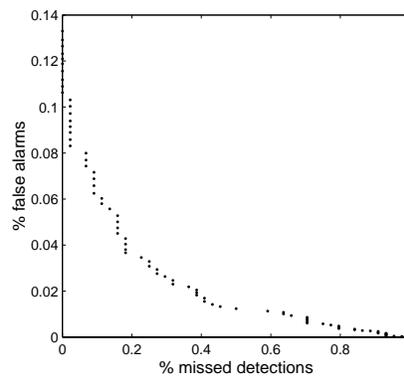
Figure 14. The ROC curve for the maximum probabilistic transition in Fig. 10

.

probability transition region in Fig. 10. Two issues with taking an actual time series and using the monitoring scheme above is that it may miss an outbreak that is there (missed detection), or it may predict an outbreak that does not occur. These statistics depend heavily on the size of the monitoring one uses. To see this in Fig. 14, we change the radius around of the center of the bull's eye and the radius around it's preimage. Each dot plotted in Fig. 14 is for a different radius. The smallest radii are represented by the data points on the right. As we increase the radii, the data points move along the curve to the left. The false alarms are those outbreaks predicted by the bull's eye, but do not occur. The missed detection are the bursts that occur but are not predicted by the maximum flux hypothesis. It is the percentage not detected.

Given that the class of population models considered here are in wide use today for modeling epidemics and lasers, it is possible to see how the theory presented might be used to test prediction and control schemes in a real experiment. Although the models assume a single homogeneous population, coupling lasers would allow one to consider migration of disease across several population groups of different geographic areas. It would be an excellent testbed for different epidemic control schemes in an experimental setting, where the stochastic dynamics is quite similar to the models in use today.

ACKNOWLEDGMENTS

REFERENCES

1. J. Gao and W. Tung, "Pathological tremors as diffusional processes," *Biological Cybernetics* **86**, pp. 263–270, 2002.

2. D. Rand and H. Wilson, "Chaotic stochasticity: a ubiquitous source of unpredictability in epidemics," *P. Roy. Soc. Lond. B Bio.* **246**, pp. 179–184, 1991.

3. D. Earn, P. Rohani, B. Bolker, and B. Grenfell, "A simple model for complex dynamical transitions in epidemics," *Science* **287**, pp. 667–670, 2000.

4. R. M. Anderson and R. M. May, *Infectious Diseases of Humans-DYnamics and Control*, Oxford Science Publications, 1991.

5. S. K. Hwang, J. B. Gao, and J. M. Liu, "Noise-induced chaos in an optically injected semiconductor laser model," *Physical Review E* **61**, pp. 5162–5170, 2000.

6. C. Towns, *How the laser happened- Adventures of a scientist*, Oxford University Press, New York, 1999.

7. D. Bernoulli, "Essai d-une nouvelle analyse de la mortalite causee par la petite verole et des advantages de l'inoculation pour la prevenir," *Mem. Math. Phys. Acad. Roy. Soc. Paris* , pp. 1–45, 1760.

8. W. H. Hamer, "Epidemic disease in england," *Lancet* **i**, pp. 733–9, 1906.

9. R. M. Anderson, "Populations, infectious disease and immunity-a very nonlinear world," *Phil. Trans. Royal Soc. London Series B* **346**, pp. 457–505, 1994.

10. B. M. Bolker and B. T. Grenfell, "Chaos and biological complexity in measles dynamics," *P. Roy. Soc. Lond. B Bio.* **251**, pp. 75–81, 1993.

11. B. M. Bolker, "Chaos and complexity in measles models - a comparative numerical study," *IMA J. Math. Appl. Med.* **10**, pp. 83–95, 1993.

12. I. B. Schwartz and H. Smith, "Infinite subharmonic bifurcations in an SEIR epidemic model," *J. Math. Biol.* **18**, pp. 233–253, 1983.

13. L. Billings, E. M. Bollt, D. S. Morgan, and I. B. Schwartz, "Stochastic global bifurcations in perturbed hamiltonian systems." to appear in Discrete and Continuous Dynamical Systems, 2002.

14. E. M. Bollt, L. Billings, and I. B. Schwartz, "A manifold independent approach to understanding transport in stochastic dynamical systems," *Physica D* **173**, pp. 153–177, 2002.

15. L. Billings and I. B. Schwartz, "Exciting chaos with noise: unexpected dynamics in epidemic outbreaks," *J. Math. Biol.* **44**, pp. 31–48, 2002.

16. B. T. Grenfell, B. M. Bolker, and A. Kleczkowski, "Seasonality and extinction in chaotic metapopulations," *P. Roy. Soc. Lond. B Bio.* **259**, pp. 97–103, 1995.

17. I. B. Schwartz, "Multiple stable recurrent outbreaks an predictability in seasonally forced nonlinear epidemic models," *J. Math. Biol.* **21**, pp. 347–361, 1985.

18. R. Meucci, D. Cinotti, E. Allaria, L. Billings, I. Triandaf, D. S. Morgan, and I. B. Schwartz, "Controlled and sustained chaos in a driven laser." to appear in Physica D, 2003.

19. R. Meucci, D. Cinotti, E. Allaria, L. Billings, I. Triandaf, D. Morgan, and I. B. Schwartz, "Global manifold control in a driven laser: sustaining chaos and regular dynamics," *Physica D-Nonlinear Phenomena* **189**, pp. 70–80, 2004.

20. T. W. Carr, L. Billings, I. B. Schwartz, and I. Triandaf, "Bi-instability and the global role of unstable resonant orbits in a driven laser," *Physica D* **147**, pp. 59–82, 2000.

21. M. Friedlin and A. Wentzel, *Random Perturbations in Dynamical Systems*, Springer-Verlag, Berlin, 1984.

22. A. Hamm, T. Tél, and R. Graham, "Noise-induced attracctor explosions near tangent bifurcations," *Physics Letters A* **185**, pp. 313–320, 1994.

23. M. Dykman, P. McClintock, V. Smelyanski, N. Stein, and N. Stocks, "Optimal paths and the prehistory problem for large fluctuations in noise-driven systems," *Physical Review Letters* **68**, pp. 2718–2721, 1992.

24. R. Maier and D. Stein, "Escape problem for irreversible systems," *Physical Review E* **48**, pp. 931–938, 1993.

25. N. G. van Kampen, *Stochastic processes in physics and chemistry*, North-Holland Publishing Co., Amsterdam, 1981. Lecture Notes in Mathematics, 888.

26. G. Froyland and K. Aihara, "Ulam formulae for random and forced systems," in *Proceedings of the 1998 International Symposium on Nonlinear Theory and its Applications*, **2**, pp. 623–626, (Crans-Montana, Switzerland), September 1998.

27. L. Billings, E. M. Bollt, and I. B. Schwartz, "Phase-space transport of stochastic chaos in population dynamics of virus spread," *Physical Review Letters* **88**, p. 234101, 2002.
28. L. Arnold, *Random Dynamical Systems*, Springer-Verlag, New York, 1998.